THE JOURNAL OF BIOLOGICAL CHEMISTRY VOL. 284, NO. 14, pp. 9566–9577, April 3, 2009

Mechanistic Insights into the Hydrolysis and Synthesis of Ceramide by Neutral Ceramidase*[S]

Received for publication, October 28, 2008, and in revised form, December 8, 2008 Published, JBC Papers in Press, December 16, 2008, DOI 10.1074/jbc.M808232200

Tsuyoshi Inoue[‡1,2], Nozomu Okino[§¶1], Yoshimitsu Kakuta[§], Atsushi Hijikata[‖], Hiroyuki Okano[‡], Hatsumi M. Goda[§], Motohiro Tani[§3], Noriyuki Sueyoshi[§4], Kouji Kambayashi[‡], Hiroyoshi Matsumura[‡], Yasushi Kai[‡5], and Makoto Ito[§¶6]

From the [‡]Department of Applied Chemistry, Graduate School of Engineering, Osaka University, 2-1 Yamada-Oka, Suita, Osaka 565-0871, Japan, the [§]Department of Bioscience and Biotechnology, Graduate School of Bioresource and Bioenvironmental Sciences, Kyushu University, 6-10-1 Hakozaki, Higashi-ku, Fukuoka 812-8581, Japan, the [‖]Laboratory for Immunogenomics, RIKEN Research Center for Allergy and Immunology, 1-7-22 Suehiro-cho, Tsurumi-ku, Yokohama 230-0045, Japan, and the [¶]Core Research for Evolutional Science and Technology, Japan Science and Technology Agency, 5 Sanbancho, Chiyoda-ku, Tokyo 102-0075, Japan

Ceramidase (CDase; EC 3.5.1.23) hydrolyzes ceramide to generate sphingosine and fatty acid. The enzyme plays a regulatory role in a variety of physiological events in eukaryotes and also functions as an exotoxin in particular bacteria. The crystal structures of neutral CDase from *Pseudomonas aeruginosa* (PaCD) in the C2-ceramide-bound and -unbound forms were determined at 2.2 and 1.4 Å resolutions, respectively. PaCD consists of two domains, and the Zn^{2+}- and Mg^{2+}/Ca^{2+}-binding sites are found within the center of the N-terminal domain and the interface between the domains, respectively. The structural comparison between the C2-ceramide-bound and unbound forms revealed an open-closed conformational change occurring to loop I upon binding of C2-ceramide. In the closed state, this loop sits above the Zn^{2+} coordination site and over the opening to the substrate binding site. Mutational analyses of residues surrounding the Zn^{2+} of PaCD and rat neutral CDase revealed that the cleavage or creation of the *N*-acyl linkage of ceramide follows a similar mechanism as observed for the Zn^{2+}-dependent carboxypeptidases. The results provide an understanding of the molecular mechanism of hydrolysis and synthesis of ceramide by the enzyme. Furthermore, insights into the actions of PaCD and eukaryotic neutral CDases as an exotoxin and mediators of sphingolipid signaling are also revealed, respectively.

Ceramide (*N*-acylsphingosine; Cer)[7] is a central metabolite of sphingolipids and is involved in the regulation of a wide spectrum of physiological events, including cell growth, differentiation, apoptosis, and exocytosis (1, 2). Sphingosine (Sph) and Sph 1-phosphate (S1P), the metabolites of Cer, mediate cell proliferation, survival, adhesion, and motility, through the modulation of cytosolic protein kinases (3) and the activation of the G-protein-coupled receptors ($S1P_{1-5}$) (4, 5). Consequently, the balance of the cellular contents of Cer/Sph/S1P is thought to regulate a diverse array of cellular responses.

Ceramidase (CDase; *N*-acylsphingosine amidohydrolase; EC 3.5.1.23) is an enzyme that catalyzes the hydrolysis of the *N*-acyl linkage of Cer to generate Sph and fatty acid (6). The enzyme was also found to catalyze the reverse hydrolysis reaction that condenses fatty acid to Sph, generating Cer (6, 7); however, the biological significance of the reverse reaction is unknown (7, 8). Since Sph is not produced through *de novo* synthesis (9), CDase activity is considered to be a rate-limiting factor in determining the intracellular levels of Sph and possibly S1P. S1P is produced from Sph by Sph kinase (10). Three distinct families (acid, neutral, and alkaline CDases) are grouped based on their optimal pH and primary structures (11). Neutral CDase (nCDase), showing an optimal pH of 6.5–8.5, was first found (12) and cloned (13) in *Pseudomonas aeruginosa*, and subsequently cloned from slime mold (14), fruit flies (15), zebrafish (16), mice (17, 18), rats (19), and humans (20, 21). Despite the high sequence similarity between the nCDases, only the slime mold enzyme exhibits maximal enzymatic activity at approximately pH 3 (14). The structural basis for this discrepancy remains to

* This work was supported in part by CREST-JST (to M. I. and N. O.), Basic Research B 18380061 (to M. I.), and Grant-in-Aid for Young Scientists B 19770086 (to N. O.) from the Japanese Ministry of Education, Culture, Sports, Science, and Technology. The costs of publication of this article were defrayed in part by the payment of page charges. This article must therefore be hereby marked "*advertisement*" in accordance with 18 U.S.C. Section 1734 solely to indicate this fact.

[S] The on-line version of this article (available at http://www.jbc.org) contains supplemental Figs. 1–3.

The atomic coordinates and structure factors (codes 2ZWS and 2ZXC) have been deposited in the Protein Data Bank, Research Collaboratory for Structural Bioinformatics, Rutgers University, New Brunswick, NJ (http://www.rcsb.org/).

[1] Both of these authors contributed equally to this work.

[2] To whom correspondence may be addressed. E-mail: inouet@chem.eng.osaka-u.ac.jp.

[3] Present address: Dept. of Chemistry, Faculty of Science, Kyushu University, 6-10-1 Hakozaki, Higashi-ku, Fukuoka 812-8581, Japan.

[4] Present address: Dept. of Life Sciences, Faculty of Agriculture, Kagawa University, Ikenobe 2393, Miki-cho, Kagawa 761-0795, Japan.

[5] Present address; Dept. of Environmental and Biotechnological Frontier Engineering, Fukui University of Technology, Gakuen 3-6-1, Fukui 910-8505, Japan.

[6] To whom correspondence may be addressed. E-mail: makotoi@agr.kyushu-u.ac.jp.

[7] The abbreviations used are: Cer, ceramide; CDase, ceramidase; nCDase, neutral ceramidase; PaCD, ceramidase from *P. aeruginosa*; Sph, sphingosine; S1P, sphingosine 1-phosphate; GOL, glycerol; NBD, 4-nitrobenzo-2-oxa-1,3-diazole; PlcH, hemolytic phospholipase C from *P. aeruginosa*; SeMet, selenomethionine-substituted.

be elucidated. nCDases from bacteria, *Drosophila*, and slime mold are secreted proteins (13–15), whereas mammalian and zebrafish enzymes are type II integral membrane proteins, which occasionally detach from the cells after processing of the N-terminal region (16, 22). This discrepancy was shown to depend on the presence of a mucin-like domain (mucin box) near the N terminus that is highly glycosylated with *O*-glycans (22). The vertebrate enzymes possess the mucin box, whereas this motif is absent in the bacteria and invertebrate enzymes. The cellular location of the enzyme may influence the function of the protein. In contrast to the N-terminal region, the C-terminal tail of nCDase is strictly conserved through bacteria to humans and is indispensable for the correct folding, localization, and enzyme activity; however, the molecular basis is poorly understood (23).

Several lines of evidence indicate the biological and physiological functions of nCDases. Recently, we reported that *P. aeruginosa* hemolytic phospholipase C (PlcH) and CDase (PaCD) were induced simultaneously by membrane lipids, such as sphingomyelin and Cer. The hemolysis of human erythrocytes caused by PlcH was significantly enhanced by the nCDase. This is due to the conversion of Cer to Sph in the plasma membranes (24). Acharya *et al.* (25–27) reported that the nCDase of *Drosophila* is integral to maintain photoreceptor functions and homeostasis, and a null mutation of the nCDase was lethal (28). We found that a knockdown of the zebrafish nCDase gene resulted in a defect of blood cell circulation during embryogenesis (16). The physiological importance of nCDase is explained in part by data showing that the enzyme is involved in Cer metabolism at the plasma membrane and in the extracellular milieu and possibly regulates S1P-mediated signaling (29). Kono *et al.* (30) generated nCDase-null mice that were viable and did not show obvious abnormality. This is possibly due to the compensation by another class of CDases. However, intestinal degradation of sphingolipids by the null mice was impaired, suggesting that nCDases expressed in the intestine are essential for the digestion of dietary Cer.

We report here the crystal structure of PaCD, which shows that the overall fold consists of two domains: a novel catalytic domain and an immunoglobulin fold domain. The x-ray crystal structure and mutation analyses of the PaCD revealed that the enzyme catalyzes the reversible reaction, in which the *N*-acyl linkage of Cer is cleaved or created, by a zinc-dependent mechanism. This mechanism is similar to zinc-dependent carboxypeptidases. Finally, the present study provides insights into the hydrolysis of Cer by nCDases, which may function as an exotoxin in bacteria, and modulate sphingolipid-mediated signaling in eukaryotes.

EXPERIMENTAL PROCEDURES

Materials—D-*erythro*-Sph and Triton X-100 were purchased from Sigma. Sphingomyelinase from *Bacillus cereus* was obtained from Funakoshi (Tokyo, Japan). C12-NBD-fatty acid was purchased from Invitrogen. C12-NBD-Cer was prepared by a method reported previously (12). A precoated Silica Gel 60 TLC plate was purchased from Merck. All other reagents were of the highest purity available.

Assay for the Hydrolysis Reaction of CDase—PaCD and rat nCDase activities were measured using C12-NBD-Cer as the substrate, as described previously (12). Briefly, the reaction mixture contained 1 nmol of C12-NBD-Cer and an appropriate amount of the enzyme in 20 μl of 25 mM Tris-HCl buffer, pH 8.5, containing 0.25% (w/v) Triton X-100 and 2.5 mM $CaCl_2$ for PaCD or 25 mM Tris-HCl buffer, pH 7.5, containing 1.0% (w/v) sodium cholate for rat nCDase. Following incubation at 37 °C, the reaction was terminated by adding 50 μl of chloroform/methanol (2:1, v/v), mixed, and centrifuged at 16,000 $\times$ *g* for 1 min. Five microliters of the lower phase was applied to a TLC plate, which was developed with chloroform, methanol, and 25% ammonia (14:6:1, v/v/v) as the developing solvent. One enzyme unit of CDase was defined as the amount capable of catalyzing the release of 1 μmol of C12-NBD-fatty acid/min from the C12-NBD-Cer. A value of 10^{-3} units of enzyme was expressed as 1 milliunit in this study.

Assay for the Reverse Reaction of CDase—Reverse hydrolysis reaction of PaCD and rat nCDase was measured using C12-NBD-fatty acid and Sph as substrates. The reaction mixture contained 1 nmol of C12-NBD-fatty acid, Sph, and an appropriate amount of the enzyme in 20 μl of 25 mM Tris-HCl buffer, pH 7.5, containing 0.05% (w/v) Triton X-100 and 2.5 mM $CaCl_2$ (in the case of rat nCDase, $CaCl_2$ was excluded). Following incubation at 37 °C for an appropriate time, the reaction was terminated by the addition of 50 μl of chloroform/methanol (2:1, v/v), mixed, and centrifuged at 16,000 $\times$ *g* for 1 min. Five microliters of the lower phase was applied to a TLC plate, which was developed with chloroform, methanol, and 25% ammonia (14:6:1, v/v/v) as the developing solvent. One enzyme unit of CDase was defined as the amount capable of catalyzing the production of 1 μmol of C12-NBD-Cer/min from the C12-NBD-fatty acid and Sph. A value of 10^{-3} units enzyme was expressed as 1 milliunit in this study.

Hemolysis Assay—The hemolytic activity was examined using sheep erythrocytes. The reaction mixture contained *B. cereus* sphingomyelinase, PaCD, 0.5% bovine serum albumin, and 5% sheep erythrocytes in Tris-buffered saline. Following incubation at 37 °C for 20 min, the reaction mixture was centrifuged at 1000 $\times$ *g* for 1 min. The supernatant was diluted with distilled water (3 volumes), and the release of hemoglobin was measured using a spectrophotometer at 490 nm.

Expression and Purification of Recombinant CDase—The PaCD expression vector (pETCDT7) was constructed by PCR using a sense primer with a NheI restriction site and T7 tag (5′-AAGCTAGCATGACTGGTGGACAGCAAATGGGTATGTCACGTTCCGCATTCACCG-3′), an antisense primer with a XhoI restriction site (5′-TTTCTCGAGGGGAGTGGTGCCGAGCACCTC-3′), and pETCD11 (13) as a template. After the amplification, the PCR product was subcloned into pET23a using NheI and XhoI restriction sites. The resulting plasmid (pETCDT7) was used for expression of PaCD. *Escherichia coli* strain BL21(DE3)pLysS cells transformed with pETCDT7 were grown at 37 °C for 12 h in 5 ml of Luria-Bertani medium supplemented with 100 μg/ml carbenicillin and 35 μg/ml chloramphenicol with shaking. The culture was transferred into 200 ml of the medium and incubated at 25 °C for 16 h with shaking. The cells were harvested by centrifugation

(8000 × *g* for 10 min) and suspended in 20 ml of 10 mM Tris-HCl buffer, pH 7.4, containing 0.15 M NaCl and 0.1% Triton X-100. After sonication for 1 min, cell debris was removed by centrifugation (8000 × *g* for 10 min). The supernatant was loaded onto a column of Ni-Sepharose 6 Fast Flow (GE Healthcare), and the column was washed with 20 mM phosphate buffer, pH 7.4, containing 0.15 M NaCl, 0.05% Triton X-100, and 40 mM imidazole. The enzyme was eluted from the column with 20 mM sodium phosphate buffer, pH 7.4, containing 0.15 M NaCl, 0.05% Triton X-100, and 200 mM imidazole. Finally, the fractions containing active protein were pooled and loaded onto a Superdex 200 HR column (GE Healthcare) equilibrated with 25 mM HEPES buffer, pH 7.5, containing 100 mM NaCl.

Expression of Rat nCDase in HEK 293 Cells—HEK293, human embryonic kidney cells, were cultured in Dulbecco's modified Eagle's medium supplemented with 10% fetal bovine serum and 60 μg/ml of kanamycin in a humidified incubator containing 5% CO_2. cDNA transfection was carried out using Lipofectamine and PLUS reagent (Invitrogen) according to the instructions of the manufacturer. At 24 h after transfection, the treated cells were scraped off and collected by centrifugation. The cell pellets were rinsed with Tris-buffered saline, suspended in lysis buffer (Tris-buffered saline containing 0.1% Triton X-100 and 3.3 μg/ml leupeptin and pepstatin), and then lysed by sonication. The obtained cell lysates were used for a CDase assay.

Preparation of Selenomethionine-substituted (SeMet) PaCD—The plasmid for overexpression of PaCD (pETCDT7) was used to transform *E. coli* B834(DE3)pLysS cells (Novagen). Transformed cells were initially precultured in LB medium containing 50 μg/ml ampicillin and 35 μg/ml chloramphenicol until the A_{600} reached 0.6. Cells were then grown at 25 °C in a modified minimal medium comprising 0.5% (w/w) glucose, 1 μM $MgSO_4$, 40 mg/ml each amino acid except methionine, 0.5 mg/ml each of the nucleic acids, 25 mg/ml selenomethionine, 50 μg/ml ampicillin, and 35 μg/ml chloramphenicol. When the A_{600} reached 0.6, 1 mM isopropyl 1-thio-β-D-galactopyranoside was added to induce protein expression, and cultivation was continued at 18 °C for an additional 8.5 h. Cells were harvested, and the SeMet protein was purified as described for the native protein, except that *n*-dodecyl-β-D-maltoside replaced Triton X-100.

Crystallization—PaCD crystals were obtained by the hanging drop method at 20 °C with a precipitant solution consisting of 0.2 M ammonium formate and 14% polyethylene glycol 3350. The native crystals, which were used for the final structure refinement, appeared after 2–3 days in 1 + 1-μl (protein + precipitant) drops using a 7 mg/ml protein solution. Crystal mother liquor containing 20% (v/v) glycerol was used as the cryoprotectant (cryo)solution.

The crystals of SeMet PaCD were also obtained by the hanging drop method at 20 °C with a precipitant solution consisting of 200 mM tripotassium citrate, 150 mM NaCl, and 18% polyethylene glycol 3350. The SeMet crystals appeared after 2–3 days in 1 + 1-μl (protein + precipitant) drops using a 5 mg/ml protein solution. Crystal mother liquor containing 20% (v/v) MPD was used as cryosolution. The complex crystals with C2-Cer were prepared using the soaking method in the presence of 10 mM C2-Cer using the crystals obtained from the same condition for SeMet PaCD.

Data Collection—All crystals were frozen in liquid nitrogen after 1–2 min in cryosolution, and data collection was performed at 100 K. SPring-8 beamline BL41XU (Harima, Japan) and the Photon Factory beamline BL5A (Tsukuba, Japan) were used as x-ray sources for the single-wavelength anomalous dispersion experiment and the native data collection, respectively. All diffraction data were processed using HKL2000 (31) and the CCP4 program suite (32). Data statistics are listed in Table 1.

Structure Determination—The initial phases were estimated by the single-wavelength anomalous dispersion method using the SeMet data. Phase calculation and density modification were processed using the program SOLVE (33) and RESOLVE (34). An initial model was built using the program ARP/wARP (35) and Coot (36). The model was refined with CNS (37). Phasing of two native structures was carried out by molecular replacement using MOLREP (38) and the SeMet-derivative model as a search model. The models were refined by CNS (37) and REFMAC (39). After several rounds of manual rebuilding and refinement, the individual B factors were refined, along with the addition of solvent molecules. The final refinement statistics are shown in Table 1. Secondary structures were assigned with DSSP (40).

Site-directed Mutagenesis—The following primers were designed to introduce the mutations into the *cdase* gene (the mutated regions are underlined): for H99A, 5′-CGGACCGGAGGCGGTGTGGGTGGCGGCGAG-3′; for R160A, 5′-CAGGTGCGACAGCAGCGAGGCGTTGCGGCTGGCGTTGCGCAG-3′; for Y460A, 5′-GCCCAGGAAGCCGAAGGCGGCTCGACCCTC-3′. The mutations were introduced by the megaprimer method (41), using the combination of the T7 NheI primer (5′-ATGGCTAGCATGACTGGTGGACAGCAAATG-3′), the C-terminal XhoI primer (5′-GGTGCTCGAGGGGAGTGGTGCCGAGCAC-3′), and one of the mutagenic primers. The final PCR products were cloned into pET23b to obtain the plasmids pETCDH99A, pETCDR160A, and pETCDY460A. H97A, H97A/H99A, and Y448A mutants were generated by the PrimeSTAR mutagenesis basal kit (Takara Bio) according to the instructions provided by the manufacturer. The following primer sets were designed to introduce the mutations into the *cdase* gene (the mutated regions are underlined): for H97A, 5′-GCCACCGCCACCCACTCCGGTCCGGG-3′ (sense) and 5′-GTGGGTGGCGGTGGCGGCGAGCATCACG-3′ (antisense); for H97A/H99A, 5′-ACCGCCACCGCCTCCGGTCCGGGCGGCTTC-3′ (sense) and 5′-GGAGGCGGTGGCGGTGGCGGCGAGCATCACG-3′ (antisense); for Y448A, 5′-GCCAGCGCCGTCACCACCCGCGAGGAA-3′ (sense) and 5′-GGTGACGGCGCTGGCATAGGCATTCGCGTA-3′ (antisense). In the case of the Ala substitution for the Glu-411 residue, PCR was performed using the T7 promoter primer, E411A (5′-GCGGATCCGCACCCCGGCCATCACGGTGAACGCGGCGGGGGCGCCGAG-3′), and pETCDT7 as a template. The E411A primer contained a BamHI site (double underlined). The resulting 1.3-kb PCR product was digested with NheI and BamHI and cloned into pETCDT7. H177A, R238A, and Y560A mutants of rat nCDase were also generated by the

TABLE 1
Summary of collected data and refinement statistics

Crystal	SeMet CDase	Unbound form	Bound form
Data collection			
Detector	SPring-8 BL41XU	PF BL5A	SPring-8 BL41XU
Wavelength (Å)	0.979	1.000	1.000
Space group	$P3_121$	$C2$	$P2_12_12_1$
Resolution range	50.0–2.60 (2.70–2.60)	50.0–1.40 (1.45–1.40)	50.0–1.98 (2.05–1.98)
Cell parameters (Å)	$a = b = 97.74$, $c = 153.17$	$a = 182.18$, $b = 59.29$, $c = 70.98$, $\beta = 102.16°$	$a = 65.74$, $b = 65.80$, $c = 340.34$
No. of reflections (measured/unique)	431,459/26,675	447,627/131,655	462,060/103,094
Redundancy (all/shell)	15.9/16.2	3.4/1.9	4.5/4.1
R_{sym} (%) (all/shell)[a]	10.2/44.6	10.2/62.1	14.4/42.0
Completeness (%) (all/shell)	100.0/100.0	90.8/51.4	97.5/93.6
Refinement statistics			
Resolution range (Å)		22.60–1.40	50.0–2.20
No. of reflections (working set/test set)		125,017/6630	70,098/3738
Completeness (%)		90.7	96.8
R_{cryst} (%)[b]/R_{free} (%)[c]		17.4/20.6	20.2/22.2
Root mean square deviations			
Bond length (Å)		0.012	1.276
Bond angles (degrees)		1.652	2.101
No. of atoms/Average B-factor (Å^2)		5236/18.8	9924/28.2
Water molecules		653/34.0	947/38.2
Zn^{2+} ion		1/14.8	2/21.1
Mg^{2+} ion		1/13.1	2/26.8
Formic acid		3/23.9	7/49.8
Palmitic acid		9/46.6	
Glycerol		18/40.7	
DMSO			2/69.1
C2-Cer			2/58.2
Ramachandran analysis			
Most favored (%)		88.2	85.1
Allowed (%)		9.0	12.7
Generously allowed (%)		2.4	1.9
Disallowed (%)		0.4	0.3

[a] $R_{sym} = \Sigma(I - \langle I\rangle)/\Sigma\langle I\rangle$, where I is the intensity measurement for a given reflection, and $\langle I\rangle$ is the average intensity for multiple measurements of this reflection.
[b] $R_{cryst} = \Sigma|F_o - F_c|\Sigma F_o$, where F_o and F_c are observed and calculated structure factor amplitudes.
[c] R_{free} value was calculated for R_{cryst}, using only an undefined subset of reflection data (5.1%).

PrimeSTAR mutagenesis basal kit. The following primer sets were designed to introduce the mutations into the rat nCDase gene (the mutated regions are underlined): for H177A, 5′-CACACTGCCTCTGGCCCAGCAGGATTT-3′ (sense) and 5′-GCCAGAGGCAGTGTGAGTGGCACTCAGGAT-3′ (antisense); for R238A, 5′-ATCAACGCCAGTCCCTCCTCTTACCTTC-3′ (sense) and 5′-GGGACTGGCGTTGATCTGCACATTAGCAACATT-3′ (antisense); for Y560A, 5′-ACCCATGCCATTACCACATATGAAGAATAC-3′ (sense) and 5′-GGTAATGGCATGGGTATAAACATTGCTCAG-3′ (antisense). After confirmation of the desired mutations by DNA sequencing, the mutant enzymes were expressed and purified by the methods described above.

Metal Analysis—Purified PaCD was dialyzed against water for 12 h at 4 °C. The quantification of metals in the sample was performed using an inductively coupled plasma mass spectrometer (model 7500C; Agilent Technologies, Inc., Palo Alto, CA).

Homology Modeling of nCDase Homologues—The homology models of human, mouse, rat, zebrafish, *Dictyostelium discoideum*, fruit fly, and *Mycobacterium tuberculosis* nCDases were built using MODELLER 9v1 (42) and were based on the crystal structure of PaCD. The sequence alignment of the nCDases was obtained using ClustalW (43) with manual adjustment performed to take into account structural positions of insertions and deletions. The model structures were evaluated with the discrete optimized protein energy method (44) implemented in the MODELLER package.

RESULTS

The Overall Structure of Substrate-unbound PaCD—The crystal structure of the substrate-unbound form has been determined at 1.4 Å resolution. Of the 645 residues, 15 residues in a loop region (positions 329–343) near the active site were not constructed because of poor electron density in this region.

The structure consists of two domains (Fig. 2). The structure of the N-terminal domain consists of three β-sheets composed of 12 β-strands. The three β-sheets form a β-prism fold at the center, which is surrounded by six long α-helices and five additional short α-helices. Each of the β-sheets, I, II, or III, consists of four β-strands: β-sheet I, S1 (residues 5–13), S4 (residues 41–49), S5 (residues 55–61), and S6 (residues 91–95); β-sheet II, S8 (residues 142–152), S10 (residues 161–189), S11 (residues 194–200), and S13 (residues 238–242); β-sheet III, S16 (residues 295–303), S20 (residues 392–400), S21 (residues 403–408), and S23 (residues 435–439).

In contrast, the C-terminal domain consists of two β-sheets composed of eight β-strands, forming a β-sandwich fold (Figs. 1 and 2). β-Sheet IV consists of four β-strands (S27 (residues 539–545), S31 (residues 595–603), S30 (residues 584–591), and S3 (residues 32–36)) from the N-terminal domain, whereas β-sheet V consists of the four β-strands (S29 (residues 574–578), S28 (residues 560–566), S32 (residues 611–622), and S33 (residues 629–634)) (Figs. 1 and 2).

The program DALI (45, 46) (available on the World Wide Web) indicated that the N-terminal domain of PaCD has no structural similarity with other protein structures in the Protein

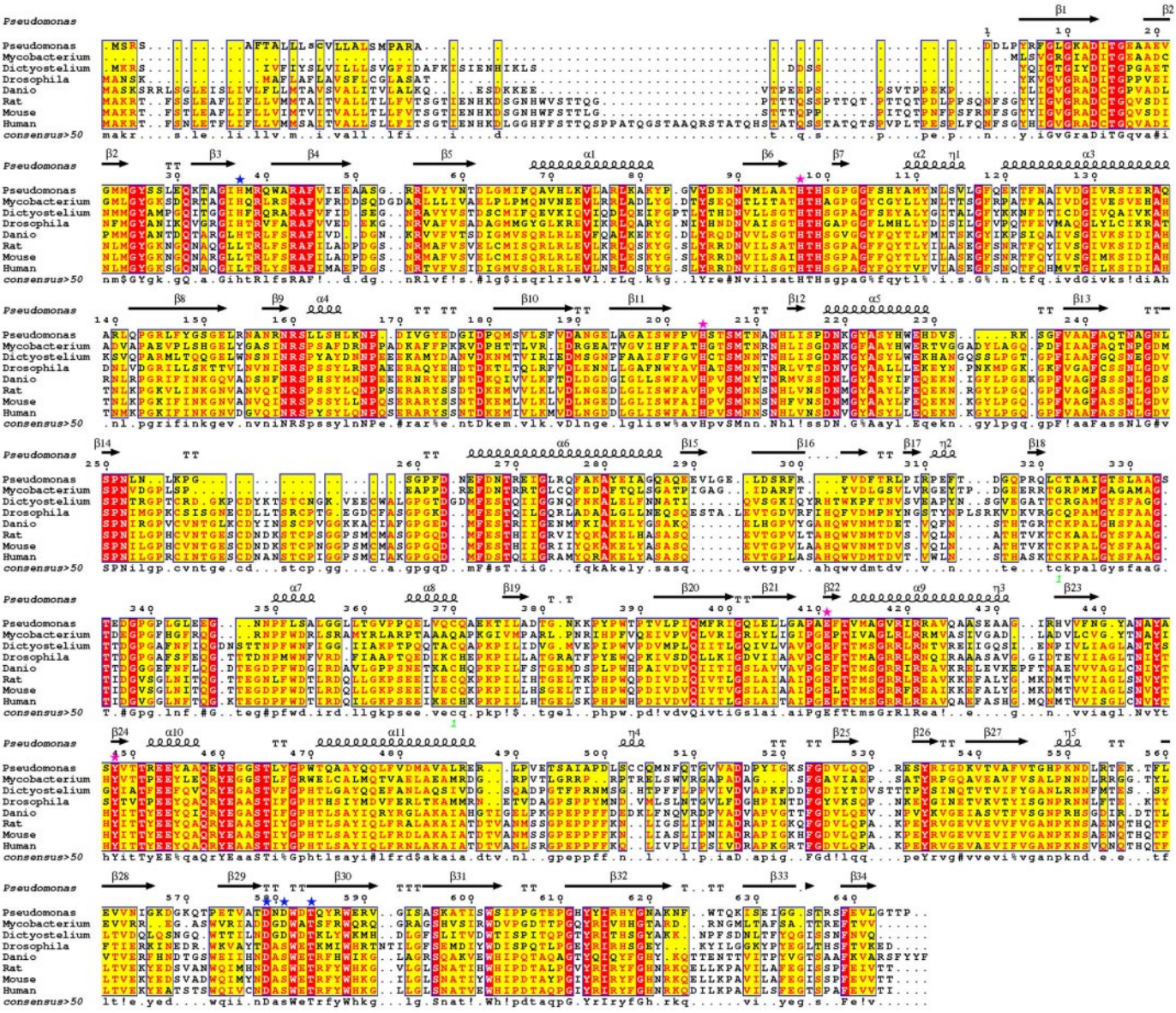

FIGURE 1. **Multiple sequence alignments of PaCD against other nCDases.** The sequences of nCDases from *M. tuberculosis*, slime mold (*D. discoideum*), fruit flies (*Drosophila melanogaster*), zebrafish (*Danio rerio*), rats (*Rattus norvegicus*), mice (*Mus musculus*), and humans (*Homo sapiens*) were aligned against the sequence of PaCD. *Red-shaded* residues are conserved in all nCDases, whereas *yellow-shaded* amino acids are similar residues. The secondary structure elements of PaCD are shown *above* the PaCD sequence. The residues participating in the Zn^{2+}-binding site and the Mg^{2+}/Ca^{2}-binding site are shown by *red stars* and *blue stars*, respectively, while those for the disulfide bond are shown in green numbers.

Data Bank, whereas the architecture of the C-terminal domain is similar to members of the β-sandwich fold. The structure was 54 (height) × 80 (width) × 48 (depth) Å in size, and the two domains are linked by the coordination of a metal ion. The electrostatic potential map shows that PaCD possesses two acidic regions where metal ions are coordinated (Fig. 2*C*).

The Metal Binding Sites of PaCD—The crystallization conditions contained 100 mM Mg^{2+} to increase the reproducibility of the crystals. The high resolution structure of PaCD showed the presence of an Mg^{2+}/Ca^{2+} binding site. This metal binding site was constructed by the residues from the turn structure between S29 (residues 574–578) and S30 (residues 584–591) and those from S3 (residues 32–36) in the N-terminal domain, forming an octahedral structure (Fig. 2*D*). Mg^{2+} may stabilize the interaction between the two domains by connecting the two β-sheets of the C-terminal domain to the His-37 carbonyl group in the N-terminal domain.

On the other hand, inductively coupled plasma mass spectrometry of PaCD indicated the presence of zinc at 0.83 mol/mol protein. Other metals, including magnesium, calcium, manganese, and copper, were not detected in recombinant PaCD. This result indicates that PaCD contains ~1 mol of zinc/mol of protein. The high resolution x-ray analysis of PaCD showed the presence of bound Zn^{2+} centered on the top face of the β-prism. Zn^{2+} was coordinated by two histidine residues, one glutamate, one tyrosine, and a water molecule, forming an octahedral structure (Fig. 2*E* and Table 2).

The Small Molecules That Bind to the Active Site of PaCD—The high resolution electron density map of the substrate-unbound form clearly defined the location of 18 glycerol (GOL)

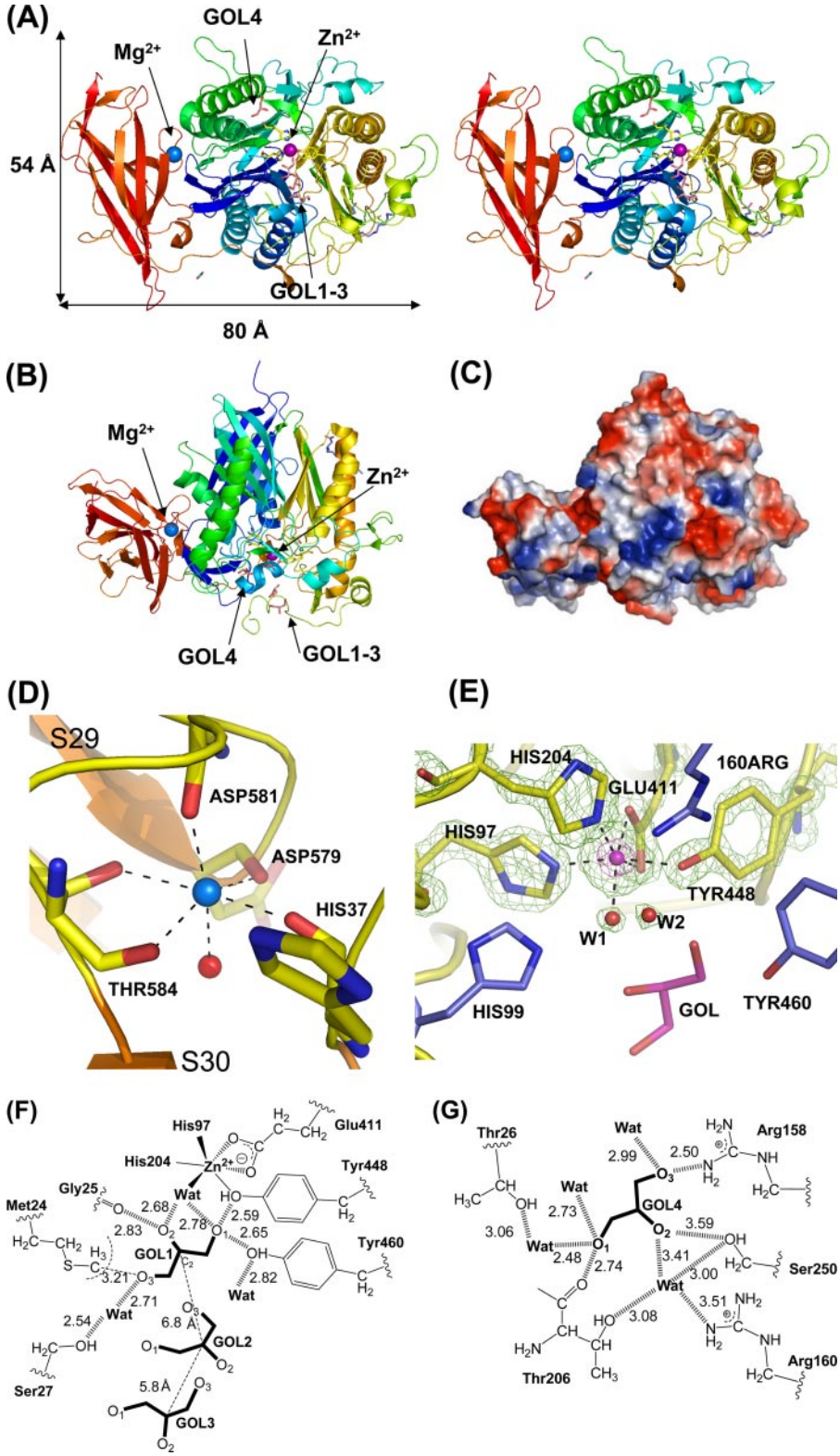

FIGURE 2. **Structure and metal binding sites of PaCD.** *A*, stereoview looking down on to the top of the core structure with a β-prism conformation consisting of three β-sheets visible. *B*, side view of the core structure. The structure is *colored* from *blue* to *red* by position in the sequence. The GOL molecules are presented as a *stick representation* with all oxygen atoms in *red* and carbon atoms for each molecule in *orange*. Only four GOL molecules of the 18 GOLs found in the structure are shown in the figures. Magnesium (*blue*) and zinc (*magenta*) ions are shown as sphere representations. *C*, the electrostatic potential of the molecular surface was calculated using GRASP (56), where *blue* represents electropositive potential >15 *kT* and *red* represents electronegative potential <-15 *kT*. The coordination structures of Mg^{2+} (*D*) and Zn^{2+} ions (*E*) are presented in a *stick representation* with carbon, oxygen, and nitrogen atoms in *yellow*, *red*, and *blue*, respectively. The contours were calculated by using the native data presented in the $2F_o - F_c$ omit map at 1.2 σ (*light green*) as well as the anomalous difference map at 4.0 σ (*magenta*). The water molecules are shown as *sphere model representations* and are *colored red*. The residues *colored* in *blue* were examined by a mutation analysis. Figures were prepared with Pymol (available on the World Wide Web). The schematic drawings with the hydrogen bond distances (Å) are shown for the GOL-bound at the active (*F*) and the remote (*G*) sites.

TABLE 2
Bond lengths and angles of the coordinated Zn^{2+} and Mg^{2+} ions

Bonds	Lengths	Bonds	Lengths
	Å		*Å*
Zn–N(His-97)	2.17	Mg-CO[a](Asp-581)	2.32
Zn–N(His-204)	2.11	Mg-CO(Asp-579)	2.62
Zn–O1(Glu-411)	2.06	Mg-N(His-37)	2.20
Zn–O2(Glu-411)	2.51	Mg-O(Thr-584)	2.30
Zn–O(Tyr-448)	2.17	Mg-CO(Thr-584)	2.48
Zn–O(W1)	2.12	Mg-O(W3)	2.54
Bonds	**Angles**	**Bonds**	**Angles**
	degrees		*degrees*
N(His-204)–Zn–N(His-97)	94.4	CO(Asp-581)–Mg–CO(Asp-579)	117.3
N(His-204)–Zn–O1(Glu-411)	94.5	CO(Asp-581)–Mg–N(His-37)	100.9
N(His-204)–Zn–O(Tyr-448)	103.5	CO(Asp-581)–Mg–O(Thr-584)	90.4
N(His-204)–Zn–O(W1)	104.9	CO(Asp-581)–Mg–CO(Thr-584)	82.8
N(His-97)–Zn–O1(Glu-411)	91.3	CO(Asp-579)–Mg–N(His-37)	81.0
O1(Glu-411)–Zn–O(Tyr-448)	90.8	N(His-37)–Mg–O(Thr-584)	96.7
O(Tyr-448)–Zn–O(W1)	83.3	O(Thr-584)–Mg–CO(Thr-584)	81.5
O(W1)–Zn–N(His-97)	88.8	CO(Thr-584)–Mg–CO(Asp-579)	99.0
O_2(Glu-411)–Zn–N(His-97)	84.3	O(W3)–Mg–CO(Asp-579)	62.9
O_2(Glu-411)–Zn–O1(Glu-411)	56.7	O(W3)–Mg–N(His-37)	88.4
O_2(Glu-411)–Zn–O(Tyr-448)	81.8	O(W3)–Mg–O(Thr-584)	89.6
O_2(Glu-411)–Zn–O(W1)	104.0	O(W3)–Mg–CO(Thr-584)	88.1

[a] CO, carbonyl oxide.

molecules, which was used as a cryoprotectant for data collection. Three GOLs (GOL1 to -3) are located in the long putative cleft of the active site (Fig. 2*A*). GOL1 is adjacent to the Zn^{2+} binding site and hydrogen-bonds to Tyr-448, Tyr-460, and the water coordinated to Zn^{2+} (Fig. 2*F*). The O2 atom of GOL1 is hydrogen-bonded to the carbonyl group of Gly-25 and the coordinated water molecule (W1), which was followed by the hydrogen bond network, including His-99, a second water molecule (W2), and Arg-160. The distances are shown in Fig. 2*F*. The two other GOL molecules, GOL2 and GOL3, are also located in the putative active site, whereas GOL4 bound at a remote site that is far from the bound GOL1 (*i.e.* 13.6 Å; Fig. 2, *A* and *G*).

Mutation Analysis around the Zn^{2+} Binding Site of PaCD and Rat CDase—Two distinct metal-binding sites, Mg^{2+}/Ca^{2+} and Zn^{2+}, were identified in the x-ray crystal of PaCD. In the Mg^{2+}/Ca^{2+} binding site, Asp-579 and Thr-584 are completely conserved among all nCDases, whereas His-37 is only conserved in the nCDases of bacteria, *Drosophila*, slime mold, and zebrafish. Asp-581 was converted to Ser-581 in the enzymes of *Drosophila* and mammals. In contrast, His-97, His-204, Glu-411, and Tyr-448 constituting the residues involved in coordination of the Zn^{2+} ion are completely conserved among all nCDases. Moreover, Gly-25, His-99, Arg-160, and Tyr-460, comprising the hydrogen bond network around the Zn^{2+} ion and recognition of the bound GOL molecule in the putative active site cleft, are conserved among all nCDases. Thus, we generated the single mutants H97A, H99A, R160A, E411A, Y448A, and Y460A and the double mutant H97A/H99A of PaCD to assess the importance of these residues for nCDase activity. Using C12-NBD-Cer as a substrate, the hydrolysis activities of the H97A, H99A, H97A/H99A, Y448A, and R160A mutants were found to be 10,000-fold less than the wild type, whereas the activities of the E411A and Y460A mutants were 523- and 1380-fold less than the wild type. The results indicate that the Zn^{2+}-binding residues His-97 and Tyr-448 are indispensable to form the metal-binding site and the active site, whereas Glu-411 may only have a role in metal coordination. In addition, His-99 and Arg-160 are residues proposed to be involved in catalysis, and Tyr-460 is involved in substrate binding. Interestingly, the reverse hydrolysis activity, which was measured using Sph and NBD-dodecanoic acid as substrates, was completely abolished in these mutants. These results clearly indicated that these seven residues surrounding the Zn^{2+} binding site are indispensable for the forward and the reverse activity of PaCD. In addition, the results suggest that the cleavage or creation of *N*-acyl linkage of Cer is conducted by the same reversible mechanism (Table 3). Furthermore, hemolytic activity of PaCD was found to be greatly reduced in these mutants (Table 3 and supplemental Fig. 1), suggesting that the hydrolysis of membrane Cer by PaCD is performed by the same reaction mechanism.

TABLE 3
The activity of wild type and mutant nCDases

CDase from *P. aeruginosa*[a]	Hydrolysis	Reverse	Increase in hemolysis
	milliunits/mg protein		
Wild type	20,240 ± 890	15,740 ± 140	+
H97A (Zn^{2+} binding)	3.01 ± 0.06	4.64 ± 0.09	−
H99A (deprotonation)	1.98 ± 0.26	1.22 ± 0.03	−
H97A/H99A (Zn^{2+} binding/deprotonation)	0.32 ± 0.02	0.35 ± 0.01	−
R160A (deprotonation)	2.28 ± 0.04	2.50 ± 0.02	−
E411A (Zn^{2+} binding)	38.7 ± 0.3	9.72 ± 0.12	−
Y448A (Zn^{2+} binding, deprotonation)	0.86 ± 0.03	0.38 ± 0.01	−
Y460A (interaction with Cer)	14.6 ± 0.4	7.32 ± 1.18	−
CDase from rat[b]	**Hydrolysis**	**Reverse**	
	microunits/mg protein		
Wild type	12,900 ± 620	5070 ± 280	
H177A (H99A)	8.44 ± 1.95	13.0 ± 2.0	
R238A (R160A)	9.44 ± 0.46	12.1 ± 0.9	
Y560A (Y448A)	10.4 ± 1.0	12.6 ± 1.9	
Mock	8.17 ± 0.28	14.4 ± 1.9	
Untransfected	6.86 ± 1.14	11.7 ± 1.9	

[a] Information in parentheses indicates the possible function.
[b] Information in parentheses indicates the corresponding residue in PaCD.

Single mutants H177A (H99A), R238A (R160A), and Y560A (Y448A) (parenthesis shows the corresponding residues in

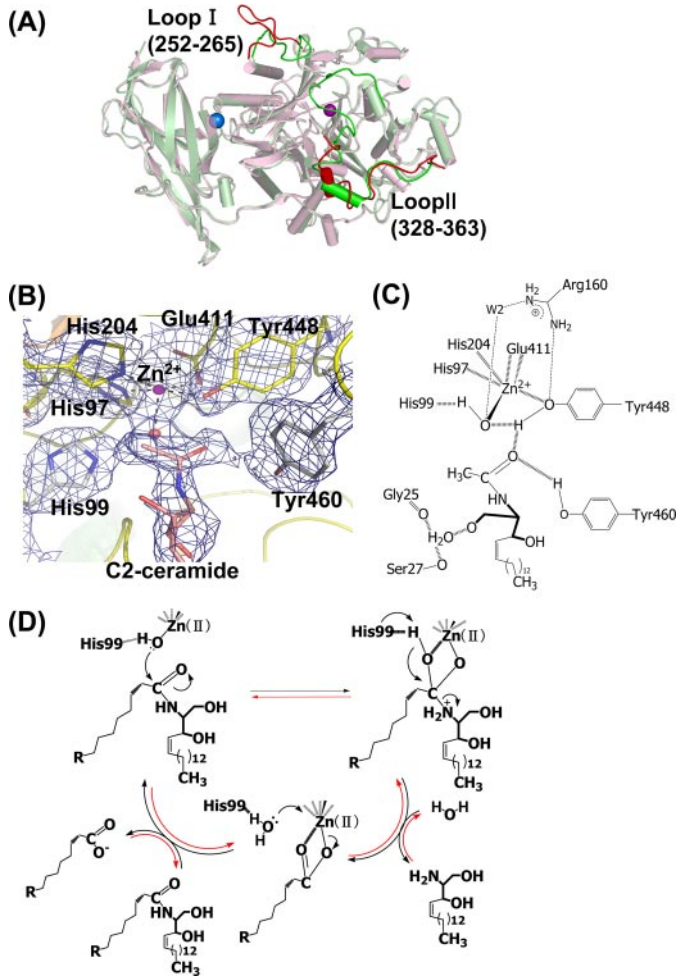

FIGURE 3. **C2-Cer bound in the putative active site of PaCD and a proposed reaction mechanism.** *A*, the structural comparison between substrate-unbound and C2 Cer-bound forms of PaCD. The substrate-unbound form is shown in *red*, whereas the C2 Cer-bound form is shown in *green*. *B*, the binding model of C2-Cer is shown as a *stick representation* with oxygen atoms in *red*, nitrogen atoms in *blue*, and carbon atoms in *yellow*. The electron density map was calculated at the 1.0 σ level. *C*, schematic drawing of the binding model of C2-Cer. The hydrogen bonds and the metal coordinate ion structure was shown by *dotted lines*. *D*, a proposed reaction mechanism of PaCD based on the structural data.

PaCD) of rat nCDase were generated. The rat nCDase activity for both forward and reverse reactions was lost for the H177A (H99A), R238A (R160A), and Y560A (Y448A) mutants (Table 3). These results indicate that the reaction mechanism of the nCDase is conserved across organisms.

The C2-Cer Complex Structure—The complex structure of PaCD·C2-Cer determined at 2.2 Å resolution was superimposed on the substrate-unbound form using the C_α carbon atoms, revealing a small r.m.s deviation of 0.496 Å; however, the noticeable conformational changes occurred on the top face above the Zn^{2+} binding site in the N-terminal domain (Fig. 3*A*). The largest movement between the corresponding atoms in the C2-Cer-bound and -unbound forms was measured for the NZ atom of Lys-256 in loop I (residues 252–264) with a value of 22 Å (Table 4). Upon binding C2-Cer, loop I undergoes a conformational change, which leads to this loop closing over the active site pocket above the Zn^{2+} binding site. Loop 329–343 was not noted in the substrate-unbound form of PaCD but was identified in loop II (residues 328–363) in the x-ray structure of PaCD

TABLE 4
Relative differences of the Cα positions of loop I between the substrate-unbound and the C2-Cer-bound forms

Loop I residue	Distance
	Å
Pro-251	0.6
Asn-252	3.9
Leu-253	2.0
Asn-254	6.6
Gly-255	11.0
Lys-256	15.2
Pro-257	15.8
Gly-258	13.1
Ser-259	9.2
Gly-260	8.1
Pro-261	4.2
Phe-262	5.6
Asp-263	2.1
Asn-264	1.0
Glu-265	0.4

bound to C2-ceramide, suggesting that the loop could also participate in the open-closed conformational change of PaCD interacting with loop I.

The C2-Cer complex structure revealed that the fatty acyl chain was located on the cavity side, whereas the sphingoid base moiety would reside on the surface side. The electron density map with the binding model of C2-Cer is shown in Fig. 3*B*. In this model, the carbonyl group of Cer replaced the O1(GOL1) atom, which was found to interact with the water molecule involved in the coordination of the Zn^{2+} ion, and hydrogen-bonded to both OH(Tyr-448) and OH(Tyr-460) with distances of 2.6 and 2.8 Å, respectively (Fig. 3, *B* and *C*). The central OH group of Cer was stabilized by both O_γ(Ser-27) and O(Gly-25) atoms via a water molecule, which regulates the orientation of the two long chains of Cer in the cavity. However, the substrate-binding model was created in the present study from an x-ray crystal structure of PaCD in a complex with the artificial substrate C2-ceramide that was not hydrolyzed by PaCD. Thus, x-ray analysis of PaCD in a complex with natural ceramide should be performed in the future to more precisely clarify the interaction between the active site of PaCD and the substrate.

PaCD hydrolyzes Cer (C18:0, d18:1) significantly faster than phyto-Cer (C18:0, t18:0) (12). The structure of the PaCD·C2-Cer complex suggests that the extra hydroxyl group of phyto-Cer faces out toward the solvent. The change in entropy as the substrate penetrates into the active site should be larger for a phyto-Cer molecule, which lacks the Cer double bond. Consequently, this change in free energy may shift to a positive value and therefore generate a larger K_m value for the binding of phyto-Cer compared with Cer.

DISCUSSION

The Proposed Reaction Mechanism of PaCD—The results of the mutagenesis and the structural analyses suggested that cleavage of the *N*-acyl linkage of Cer by nCDases proceeds by a mechanism similar to that described for zinc-dependent carboxylpeptidase (Fig. 3*D*). The first reaction step is the deprotonation of the coordinated water molecule supported by His-99 and Arg-160. The reaction starts with nucleophilic attack on the carbonyl carbon atom of Cer by the hydroxide ion produced from the coordinated water molecule. Tyr-448 and Tyr-460 may support the carbonyl oxygen atom of a substrate to reduce

the K_m value of it. The mutational analyses of these four residues proved the important role these residues play in the reaction. After the reaction, the Sph part of Cer will be released from the active site, and the remaining fatty acid will be replaced by another Cer when a new water molecule binds between His-99 and Tyr-448 and coordinates to the Zn^{2+} ion. The creation of the *N*-acyl linkage of Cer is likely to proceed via the zinc-dependent hydrolysis mechanism, but the direction of the reaction is reversed (Fig. 3*D*). This was confirmed by the findings that mutations of residues surrounding Zn^{2+} completely abolished the activity of not only the forward but also the reverse reactions of PaCD (Table 3). The x-ray structure also provides a model for the reverse reaction mechanism. Here, the active site Zn^{2+} ion associates with the carboxyl group of the fatty acid to increase the nucleophilicity, and this is followed by the nucleophilic attack of the amino group of Sph.

Moreover, the PaCD seems to hydrolyze the Cer in intact membranes by the same mechanism, because the mutation of residues surrounding the catabolic Zn^{2+} of PaCD abolished not only the hydrolytic activity toward free Cer but also the hemolytic activity toward erythrocytes (Table 3 and supplemental Fig. 1). The latter reaction strongly depends on the conversion of Cer to Sph in the plasma membranes (24). Hydrolysis of membrane-bound Cer will occur when the enzyme faces the membrane and a substrate penetrates into the remote binding site where GOL4 bound and inhibited the loop closure. Since the structure of GOL is similar to the Cer amino dialcohol scaffold, Cer will also be recognized by Thr-206, Arg-158, and Tyr-26 (Fig. 2*G*). In addition, large conformational changes in loop I and II were observed (Fig. 3*A*). These structural changes are clearly important in facilitating the binding of the substrate and catalysis.

Homology Modeling of nCDases from Different Species and the Proposed Reaction Mechanism of the nCDase Slime Mold Homologue—The primary structure of nCDase is highly conserved from bacteria to mammals. Homology models of nCDases from humans, rats, zebrafish, *Drosophila*, and *M. tuberculosis* were built using the crystal structure of PaCD as a template (supplemental Fig. 2). The three-dimensional structures of the active sites of nCDases homologues closely resembled each other, suggesting that the reaction mechanism of nCDase is shared from bacteria to mammals. The results of mutant experiments of rat nCDase (Table 3) were consistent with the modeling results. Despite the highly conserved structures of nCDases, only slime mold *D. discoideum* enzyme exhibits a maximal enzymatic activity at approximately pH 3 (14). This observation may be explained in part by comparing the three-dimensional structures between nCDase homologues. The most striking difference was observed at Glu-289 near His-132 in the *D. discoideum* enzyme, which corresponds to the Zn^{2+} ligand of His-97 in PaCD (Fig. 4). The distance between Glu-289 and His-132 was measured to be 3.5 Å, indicating the presence of a weak hydrogen bond between Glu-289 and His-132 in the *D. discoideum* enzyme (Fig. 4). In contrast, this position is an alanine in PaCD or leucine in the nCDases from humans, rats, *Drosophila*, or zebrafish (Fig. 1). Under acidic conditions, the protonation of Glu-289 could occur, and this would lead to the breaking of the hydrogen bond with the

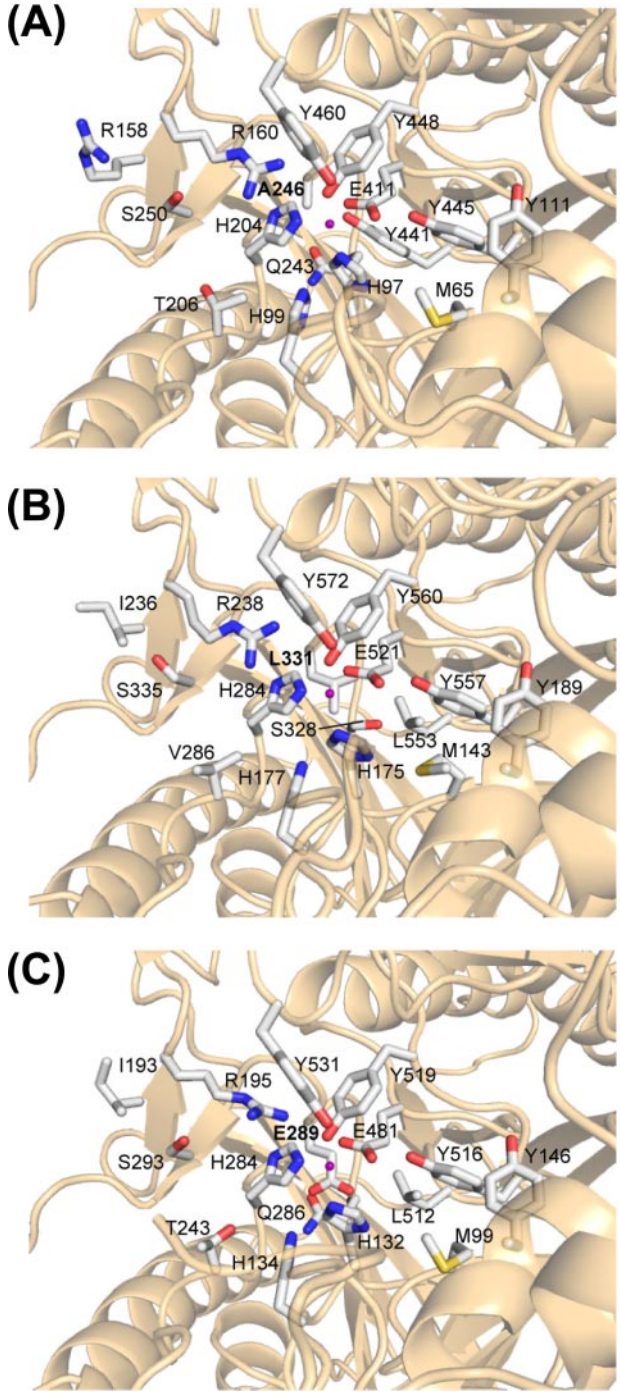

FIGURE 4. **The active site structures of PaCD and its homologues.** The active sites of the crystal structure of the PaCD (*A*) and the homology models of rat (*B*) and slime mold *D. discoideum* (*C*). The Zn^{2+} ion and the residues surrounding the active site are represented with *sphere* and *stick representations*, respectively. *White*, carbon; *red*, oxygen; *blue*, nitrogen; *yellow*, sulfur.

Zn^{2+} ligand of His-132. The loss of the hydrogen bond would lead to the formation of the Zn^{2+}-coordinated structure, which is presumably required for *D. discoideum* enzyme activity.

Mechanistic Insights into Hydrolysis of Cer at the Plasma Membrane and in the Extracellular Milieu—Two different forms, soluble or type II integral membrane, have been found in nCDases from different origins. nCDases from vertebrates (zebrafish, mice, and humans) are usually present as a type II

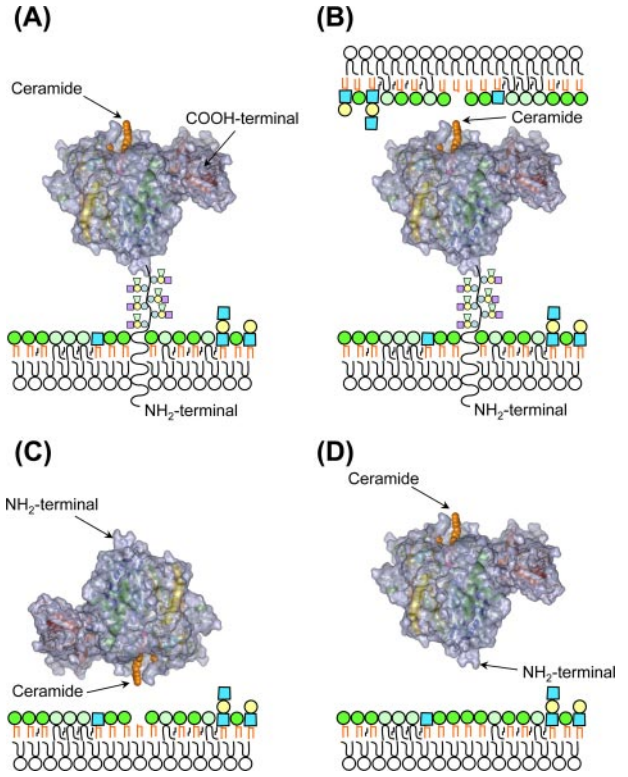

FIGURE 5. **The proposed conformations of nCDase acting on membrane-bound Cer (*B* and *C*) and free Cer (*A* and *D*).** nCDase is shown as a *ribbon model*. The type II integral membrane (*A* and *B*) and soluble (*C* and *D*) forms of nCDase are shown.

membrane protein and are occasionally found to detach from the cells after processing of the N-terminal domain (29). The nCDases from bacteria and invertebrates (*P. aeruginosa*, *Drosophila*, and slime molds) are expressed entirely as the soluble form and secreted from the cells (13–15). This discrepancy may stem from the presence of a mucin box located in the N-terminal region of the enzyme in vertebrates, which is absent in nCDases from bacteria and invertebrates. Furthermore, in contrast to the wild-type nCDase, the mucin box-deleted mutant nCDase does not remain embedded in the plasma membrane and is secreted (22).

Based on accumulating evidence and structural data obtained in this study, we propose four mechanical conformations of nCDase acting on Cer. For the integral membrane nCDase, one conformation allows the substrate binding cleft to face toward the extracellular milieu (type I; Fig. 5*A*), whereas the other allows it to face toward the plasma membrane (type II; Fig. 5*B*). For the two soluble forms, one conformation allows the substrate binding cleft to face the plasma membranes (type III; Fig. 5*C*), and in the other conformation, the active site faces toward the extracellular milieu (type IV; Fig. 5*D*). Type I and IV mechanisms involve free Cer (micellar Cer) being incorporated into the substrate-binding cavity and hydrolyzed, whereas type II and III mechanisms involve membrane-bound Cer being extracted from the membrane surface and hydrolyzed. Type I is assumed to occur on the vascular endothelial cells, where nCDase could be involved in the generation of S1P (29). This process may regulate angiogenesis and vascular maturation (29, 47). Alternatively, this type could be observed in the digestive process of food-derived Cer in the intestines where nCDase locates on the luminal surface of the villi and microvilli of absorptive epithelial cells (16, 48). Interestingly, Cer is adsorbed from the intestine after conversion to Sph with nCDase (49, 50), and nCDase-KO mice were found to be impaired in the intestinal degradation of sphingolipids (30). In type II, nCDase could hydrolyze the *trans*-located membrane-bound Cer (Fig. 5*B*), but the enzyme is not likely to hydrolyze the *cis*-located membrane Cer, because the N-terminal anchor region is not long enough to allow the cavity direct access to the *cis*-located membrane Cer. Type III could represent the action of *P. aeruginosa* exotoxin (PaCD) on membrane Cer that is generated from membrane sphingomyelin by the action of *P. aeruginosa* sphingomyelinase (PlcH) (24). PaCD significantly enhanced the PlcH-induced hemolysis due to the conversion of Cer to Sph in the plasma membranes. In *Drosophila*, nCDase seems to be integral for survival, probably because, in contrast to mammals, other classes of CDases (acid or alkaline enzyme) are not present. Since *Drosophila* CDase exists only in the soluble (15), the enzyme could circulate in the body fluid and act on membrane Cer (Fig. 5*C*) or free Cer in the extracellular milieu (Fig. 5*D*).

Significance of COOH-terminal Tails of nCDases—Despite the presence or absence of a mucin-like domain in the N-terminal region of nCDases, the C-terminal tail of the enzyme is highly conserved across all species. The x-ray structure of PaCD showed that the architecture of C-terminal domain resembles other members of the immunoglobulin superfamily (IgSF). DALI showed that the structures of invasin and cadherin are similar to that of the C-terminal domain of the nCDases with a C_α carbon r.m.s. deviation of 2.7 and 3.4 Å, respectively. Invasin binds to the host cell integrin to promote the uptake of the bacteria cells and therefore is important in infection (51), whereas cadherins mediate cell adhesion (52) and play a fundamental role in development in the presence of Ca^{2+}. The C-terminal domain of nCDases may play a role in the interaction with the plasma membranes.

The nCDases have two conserved hydrophobic residues, Phe-639 and Val-641, in the C-terminal domain. Both the V641D mutant and the deletion mutant that lacks four residues at the C-terminal end of PaCD were 10 times as sensitive to trypsin compared with the wild-type enzyme (23). Although the position of the C_α(Val-641) is far from the Mg^{2+}/Ca^{2+} and Zn^{2+} binding sites, with distances of 19 and 42 Å, respectively, the point mutation V641D may affect the structure of S5, destabilizing not only the β-sandwich fold but also the Mg^{2+}/Ca^{2+} binding site. Collectively, well conserved C-terminal tails of nCDases are indispensable for the stabilization of the protein structure.

Roles of Metal Ions in nCDases—The presence of two metal binding sites was revealed by the x-ray crystal structure of PaCD (Fig. 2, *D* and *E*). The zinc ions of PaCD and rat nCDase were shown to function as the integral catalytic metal ions. Such Zn^{2+}-dependent activity is observed for the Zn^{2+}-dependent carboxypeptidase. The activity of PaCD was completely lost in the presence of EDTA but was restored with 1 mM Ca^{2+} or Mg^{2+} (supplemental Fig. 3) (12, 13). The second metal binding (Mg^{2+} or Ca^{2+}) could be important in promoting the interaction between the two domains. Here, the metal ion pre-

sumably assists the N-terminal S3 to be included in the β-sandwich fold of the C-terminal domain. In this context, it is noteworthy that Ca^{2+} caused significant changes in the CD spectra of PaCD, and the changes were inhibited in the presence of EGTA, suggesting the binding of Ca^{2+} influenced the structure of PaCD (53). In the present study, we detected Mg^{2+}, but not Ca^{2+}, in the second binding site of crystal structure of PaCD, because high concentrations of $MgCl_2$ were used for crystallization of the enzyme. The stabilization of the structure with Mg^{2+} was indirectly proven, because crystal reproducibility/quality was reduced in the absence of Mg^{2+}. However, EDTA treatment had no effects on the activity of murine CDases. One possible explanation for this is that Mg^{2+}/Ca^{2+} binds tightly to the murine enzyme but not PaCD, and EDTA treatment is insufficient to remove the metals from the murine enzymes. It remains to be clarified whether Mg^{2+}/Ca^{2+} is present in murine enzymes after EDTA treatment.

Galadari *et al.* (54) reported the identification of a novel amidase motif in human nCDase, in which Ser-354 appears to be important for catalysis. Replacement of Ser-354 by an Ala residue caused a total loss of the enzyme activity. In the crystal model of PaCD, this serine residue is located near His-204 and Arg-160, which are residues involved in Zn^{2+}-binding and the construction of the hydrogen bond network around Zn^{2+}, respectively. The structure supports the mutagenesis study and indicates that these residues may be integral for the Zn^{2+}-dependent catalytic mechanism of the enzyme.

The hydrolysis mechanism of Cer by acid CDases seems to be different from the nCDases. Acid CDase is composed of α- and β-subunits, and cysteine-mediated self-cleavage is required for Cer hydrolysis. This observation suggests a key role of a Cys residue within the active site and may present a catalytic mechanism similar to that of the N-terminal nucleophile hydrolase family of enzymes; the members show homology to the acid CDase (55). Structural analysis of the complex with a substrate would reveal the substrate recognition mechanism in detail and therefore provide information on the binding pocket that could be utilized in structure-based drug design.

Acknowledgments—We thank Dr. Kaori Kojo for technical assistance with the preparation of the PaCD. We are indebted to Dr. Midori Watanabe (Center of Advanced Instrumental Analysis, Kyushu University) for the inductively coupled plasma mass spectrometry analysis.

REFERENCES

1. Hannun, Y. A., and Obeid, L. M. (2008) *Nat. Rev. Mol. Cell Biol.* **9,** 139–150
2. Pettus, B. J., Chalfant, C. E., and Hannun, Y. A. (2002) *Biochim. Biophys. Acta.* **1585,** 114–125
3. Hannun, Y. A., and Bell, R. M. (1987) *Science* **235,** 670–674
4. Spiegel, S., and Milstien, S. (2003) *Nat. Rev. Mol. Cell Biol.* **4,** 397–407
5. Hait, N. C., Oskeritzian, C. A., Paugh, S. W., Milstien, S., and Spiegel, S. (2006) *Biochim. Biophys. Acta.* **1758,** 2016–2026
6. Gatt, S. (1963) *J. Biol. Chem.* **238,** 3131–3133
7. Kita, K., Okino, N., and Ito, M. (2000) *Biochim. Biophys. Acta.* **1485,** 111–120
8. Okino, N., He, X., Gatt, S., Sandhoff, K., Ito, M., and Schuchman, E. H. (2003) *J. Biol. Chem.* **278,** 29948–29953
9. Merrill, A. H., Jr., and Wang, E. (1986) *J. Biol. Chem.* **261,** 3764–3769
10. Tani, M., Ito, M., and Igarashi, Y. (2007) *Cell. Signal.* **19,** 229–237
11. Ito, M., Okino, N., Tani, M., Mitsutake, S., and Kita, K. (2002) *Ceramide Signaling*, pp. 41–48, Landes BioScience Press Inc., Georgetown, TX
12. Okino, N., Tani, M., Imayama, S., and Ito, M. (1998) *J. Biol. Chem.* **273,** 14368–14373
13. Okino, N., Ichinose, S., Omori, A., Imayama, S., Nakamura, T., and Ito, M. (1999) *J. Biol. Chem.* **274,** 36616–36622
14. Monjusho, H., Okino, N., Tani, M., Maeda, M., Yoshida, M., and Ito, M. (2003) *Biochem. J.* **376,** 473–479
15. Yoshimura, Y., Okino, N., Tani, M., and Ito, M. (2002) *J. Biochem.* (*Tokyo*) **132,** 229–236
16. Yoshimura, Y., Tani, M., Okino, N., Iida, H., and Ito, M. (2004) *J. Biol. Chem.* **279,** 44012–44022
17. Tani, M., Okino, N., Mitsutake, S., Tanigawa, T., Izu, H., and Ito, M. (2000) *J. Biol. Chem.* **275,** 3462–3468
18. Tani, M., Okino, N., Mori, K., Tanigawa, T., Izu, H., and Ito, M. (2000) *J. Biol. Chem.* **275,** 11229–11234
19. Mitsutake, S., Tani, M., Okino, N., Mori, K., Ichinose, S., Omori, A., Iida, H., Nakamura, T., and Ito, M. (2001) *J. Biol. Chem.* **276,** 26249–26259
20. El Bawab, S., Roddy, P., Qian, T., Bielawska, A., Lemasters, J. J., and Hannun, Y. A. (2000) *J. Biol. Chem.* **275,** 21508–21513
21. Hwang, Y. H., Tani, M., Nakagawa, T., Okino, N., and Ito, M. (2005) *Biochem. Biophys. Res. Commun.* **331,** 37–42
22. Tani, M., Iida, H., and Ito, M. (2003) *J. Biol. Chem.* **278,** 10523–10530
23. Tani, M., Okino, N., Sueyoshi, N., and Ito, M. (2004) *J. Biol. Chem.* **279,** 29351–29358
24. Okino, N., and Ito, M. (2007) *J. Biol. Chem.* **282,** 6021–6030
25. Acharya, J. K., Dasgupta, U., Rawat, S. S., Yuan, C., Sanxaridis, P. D., Yonamine, I., Karim, P., Nagashima, K., Brodsky, M. H., Tsunoda, S., and Acharya, U. (2008) *Neuron* **57,** 69–79
26. Acharya, U., Mowen, M. B., Nagashima, K., and Acharya, J. K. (2004) *Proc. Natl. Acad. Sci. U. S. A.* **101,** 1922–1926
27. Acharya, U., Patel, S., Koundakjian, E., Nagashima, K., Han, X., and Acharya, J. K. (2003) *Science* **299,** 1740–1743
28. Rohrbough, J., Rushton, E., Palanker, L., Woodruff, E., Matthies, H. J., Acharya, U., Acharya, J. K., and Broadie, K. (2004) *J. Neurosci.* **24,** 7789–7803
29. Tani, M., Igarashi, Y., and Ito, M. (2005) *J. Biol. Chem.* **280,** 36592–36600
30. Kono, M., Dreier, J. L., Ellis, J. M., Allende, M. L., Kalkofen, D. N., Sanders, K. M., Bielawski, J., Bielawska, A., Hannun, Y. A., and Proia, R. L. (2006) *J. Biol. Chem.* **281,** 7324–7331
31. Otwinowski, Z., and Minor, W. (1993) in *Proceedings of the CCP4 Study Weekend, Data Collection and Processing*, pp. 56–62, Science and Engineering Research Council Daresbury Laboratory, Warrington, UK
32. Collaborative Computational Project 4 (1994) *Acta. Crystallogr. Sect. D. Biol. Crystallogr.* **50,** 760–763
33. Terwilliger, T. C., and Berendzen, J. (1999) *Acta. Crystallogr. Sect. D Biol. Crystallogr.* **55,** 849–861
34. Terwilliger, T. C. (2003) *Methods Enzymol.* **374,** 22–37
35. Perrakis, A., Morris, R., and Lamzin, V. S. (1999) *Nat. Struct. Biol.* **6,** 458–463
36. Emsley, P., and Cowtan, K. (2004) *Acta. Crystallogr. Sect. D Biol. Crystallogr.* **60,** 2126–2132
37. Brunger, A. T., Adams, P. D., Clore, G. M., DeLano, W. L., Gros, P., Grosse-Kunstleve, R. W., Jiang, J. S., Kuszewski, J., Nilges, M., Pannu, N. S., Read, R. J., Rice, L. M., Simonson, T., and Warren, G. L. (1998) *Acta. Crystallogr. Sect. D Biol. Crystallogr.* **54,** 905–921
38. Vagin, A., and Teplyakov, A. (2000) *Acta. Crystallogr. Sect. D Biol. Crystallogr.* **56,** 1622–1624
39. Murshudov, G. N., Vagin, A. A., and Dodson, E. J. (1997) *Acta. Crystallogr. Sect. D Biol. Crystallogr.* **53,** 240–255
40. Kabsch, W., and Sander, C. (1983) *FEBS. Lett.* **155,** 179–182
41. Sarkar, G., and Sommer, S. S. (1990) *BioTechniques* **8,** 404–407
42. Marti-Renom, M. A., Stuart, A. C., Fiser, A., Sanchez, R., Melo, F., and Sali, A. (2000) *Annu. Rev. Biophys. Biomol. Struct.* **29,** 291–325
43. Thompson, J. D., Higgins, D. G., and Gibson, T. J. (1994) *Nucleic Acids Res.* **22,** 4673–4680

44. Shen, M. Y., and Sali, A. (2006) *Protein Sci.* **15,** 2507–2524
45. Holm, L., and Sander, C. (1993) *J. Mol. Biol.* **233,** 123–138
46. Holm, L., and Sander, C. (1996) *Science* **273,** 595–603
47. Ancellin, N., Colmont, C., Su, J., Li, Q., Mittereder, N., Chae, S. S., Stefansson, S., Liau, G., and Hla, T. (2002) *J. Biol. Chem.* **277,** 6667–6675
48. Olsson, M., Duan, R. D., Ohlsson, L., and Nilsson, A. (2004) *Am. J. Physiol.* **287,** G929–G937
49. Nilsson, A. (1969) *Biochim. Biophys. Acta* **176,** 339–347
50. Ohlsson, L., Palmberg, C., Duan, R. D., Olsson, M., Bergman, T., and Nilsson, A. (2007) *Biochimie* (*Paris*) **89,** 950–960
51. Hamburger, Z. A., Brown, M. S., Isberg, R. R., and Bjorkman, P. J. (1999) *Science* **286,** 291–295
52. Nagar, B., Overduin, M., Ikura, M., and Rini, J. M. (1996) *Nature* **380,** 360–364
53. Wu, B. X., Snook, C. F., Tani, M., Bullesbach, E. E., and Hannun, Y. A. (2007) *J. Lipid Res.* **48,** 600–608
54. Galadari, S., Wu, B. X., Mao, C., Roddy, P., El Bawab, S., and Hannun, Y. A. (2006) *Biochem. J.* **393,** 687–695
55. Shtraizent, N., Eliyahu, E., Park, J. H., He, X., Shalgi, R., and Schuchman, E. H. (2008) *J. Biol. Chem.* **283,** 11253–11259
56. Nicholls, A., Sharp, K. A., and Honig, B. (1991) *Proteins* **11,** 281–296